Journal Pre-proof

Enhanced UV emission of Li–Y co-doped ZnO thin films via spray pyrolysis

O. Bazta, A. Urbieta, J. Piqueras, P. Fernández, M. Addou, J.J. Calvino, A.B. Hungría

PII: S0925-8388(19)32943-3

DOI: https://doi.org/10.1016/j.jallcom.2019.151710

Reference: JALCOM 151710

To appear in: *Journal of Alloys and Compounds*

Received Date: 4 April 2019

Revised Date: 26 July 2019

Accepted Date: 4 August 2019

Please cite this article as: O. Bazta, A. Urbieta, J. Piqueras, P. Fernández, M. Addou, J.J. Calvino, A.B. Hungría, Enhanced UV emission of Li–Y co-doped ZnO thin films via spray pyrolysis, *Journal of Alloys and Compounds* (2019), doi: https://doi.org/10.1016/j.jallcom.2019.151710.

This is a PDF file of an article that has undergone enhancements after acceptance, such as the addition of a cover page and metadata, and formatting for readability, but it is not yet the definitive version of record. This version will undergo additional copyediting, typesetting and review before it is published in its final form, but we are providing this version to give early visibility of the article. Please note that, during the production process, errors may be discovered which could affect the content, and all legal disclaimers that apply to the journal pertain.

© 2019 Published by Elsevier B.V.

Journal Pre-proof

Enhanced UV emission of Li-Y co-doped ZnO thin films via spray pyrolysis

O. Bazta[1, 3*], A. Urbieta[2], J. Piqueras[2], P. Fernández[2], M. Addou[3], J.J. Calvino[1], A.B. Hungría[1]

[1]Department of Materials Science and Metallurgical Engineering and Inorganic Chemistry, University of Cadiz, Cadiz, Spain

[2]Department of Physics, Complutense University of Madrid, Madrid, Spain

[3]Department of Physics, University Abdelmalek Essaadi FST, Tangier, Morocco

*Corresponding author address: otman.bazta@alum.uca.es

Abstract:

Pure ZnO and ZnO: 2%Y: x%Li (x=0, 3, 5 and 7 at.%) thin films have been successfully prepared onto glass substrates under optimized conditions by spray pyrolysis technique at 450 ºC and their suitability for the fabrication of efficient optoelectronic devices is demonstrated. The samples have been characterized by X-ray diffraction (XRD), Scanning electron microscopy (SEM), UV-Visible absorption spectroscopy photoluminescence (PL) and Raman spectroscopy (RS), in order to investigate the effect of Y-Li co-doping on the structure, surface morphology, and optical features of the thin films. The films crystallized into a hexagonal structure, with a preferred orientation along the c-axis. No additional phases have been observed. SEM micrographs showed that Y and Li co-doping plays a key role in the grain size and morphology of the films. The optical study via transmittance and absorption measurements within the UV-vis region revealed that the films are highly transparent (82-90%). The optical bandgap (E_g) depends on the concentration of lithium added, which is explained by the Burstein-Moss (BM) effect. The PL measurements at room temperature under excitation with 325 nm wavelength, showed an appreciable improvement of ultraviolet emission by increasing the Li co-doping concentration. This enhancement reaches a maximum at 5 at.% Li content, and decreases after further increase in Li content. Raman

Journal Pre-proof

scattering spectra were also carried out and revealed the presence of the wurtzite phase of ZnO exclusively.

Keywords: Thin films; Li-Y doped ZnO; Optical properties; luminescence; Spray pyrolysis synthesis

Introduction

Metal oxide nanostructures have gained an increasing attention in the recent years, owing to their unique properties and wide possibilities to exploit them in various applications for the development of novel devices. In particular, nanostructures of zinc oxide, a II-VI semiconductor characterized by a direct wide bandgap (3.37 eV) and large exciton binding energy of 60 meV, are considered to be attractive and promising materials for different applications in opto- and microelectronic devices [1][2][3], such as solar cells[4][5][6], UV-visible light emitting diodes (LEDs) [7],gas sensors [3-4] and photocatalysts [10][11].

In this context, different pathways have been tested to prepare and ameliorate the features of ZnO, such as Sol-gel [12][13], hydrothermal [14], Silar (Successive ionic layer adsorption and reaction) technique [15] and pulsed laser deposition [16]. To our knowledge synthesis of Li-Y co-doped ZnO thin films is reported for the first time using spray pyrolysis technique.

The structural, morphological and optical properties of ZnO can be altered by adding selected impurities to the ZnO lattice. A large number of studies have now been carried out on ZnO doped with different metallic ions, in order to achieve or improve the desired properties [17][18][19]. So far, rare earth elements and transition metals have attracted attention thanks to their excellent performance as luminescent centers. Particularly, rare earth elements are capable to enhance the optical properties of ZnO nanostructures, and among them, yttrium (Y) , is considered as an important choice [20], primarily based on the similarity between the atomic radii of both elements [21]. Thus, several reports have demonstrated the great potential of Y as a dopant to enhance the electrical and optical properties of ZnO, as well as to mitigate the deleterious effect of point defects [22][23][24]. For instance, Sharma et al [25] observed

improved crystal quality and strong near band edge (NBE) emission of Y doped ZnO nanobelts. Kaur et al[24] reported that the electrical conductivity was improved after adding an appropriate amount of Y and Li, and Yang et al reported tunable deep-level emission in Y-doped ZnO nanoparticles [26]. The addition of Li (+1) could compensate the charge unbalance provoked by the introduction of Y (+3) in the Zn (+2) sublattice. Furthermore, dual doping can be an effective way to achieve p-type conduction, enhance the solubility in the host matrix and improve other physical properties. In particular, Li has been considered to be a good candidate to obtain the desired features when co-doped with Y, owing to its potential to modify the chemical and physical properties of the ZnO matrix, and to induce p-type conductivity in ZnO. Nian et al [27] and Fujihara et al [28] have demonstrated the efficiency of Li co-doping to improve the electrical and optical properties of Al doped ZnO and Mg doped ZnO films, respectively, and Caglar et al [29] found that the crystallinity of ZnO films is enhanced by Li doping. The purpose of the present communication is to evaluate the influence of Li concentration on the structural, morphological, optical and photoluminescence properties of Y doped ZnO thin films.

Experimental details

ZnO and ZnO: 2%Y: x%Li (x=0, 3,5 and 7 at.%) thin films were deposited through spray pyrolysis method as reported for Yttrium doped films in a previous work [30]. As received zinc chloride, yttrium acetate and lithium acetate were used to prepare solutions in distilled water. A 0.05 M spray solution of zinc chloride was used as a source of zinc. The doping and co-doping were attained by adding yttrium acetate and lithium acetate at concentrations of (2 at.%) and (3, 5 and 7 at.%) respectively. Hydrochloric acid (HCl) was slowly added into the previous solution to avoid the formation of zinc hydroxide. Just before starting the deposition, the glass substrates were cleaned in 5 minutes steps in order to remove surface dirt. The first cleaning step is made with tap water with detergent, then acetone, and finally distilled water. The cleaned substrates were placed on a hot plate set at 450 °C. Thin film deposition was carried out by spraying the prepared solution onto the preheated substrates via a nozzle placed at 40 cm

Journal Pre-proof

from the hot plate during the deposition with a spray rate of 2 $ml.min^{-1}$ using compressed air as a carrier gas. After deposition, the films were left to cool down to room temperature under air and then collected for characterization.

X-ray diffraction (XRD) patterns of the films were recorded in a Bruker D8 advance X-ray diffractometer. The average crystallite size was determined by the Scherrer method from the width of the diffraction peaks. Surface morphology of the coated films was investigated via scanning electron microscopy (SEM, Nova NanoSEM 450). The optical transmission spectra were recorded in a Shimadzu UV-1603 UV-Visible spectrophotometer. The room temperature photoluminescence (PL) and Raman spectra were recorded using a confocal microscope Horiba Jobin Yvon Labram HR 800 with an excitation wavelength 325 nm and 630 nm respectively.

Results and discussion

Fig.1a shows XRD patterns of ZnO and ZnO: 2%Y: x%Li thin films. All the patterns show the main peaks of the hexagonal wurtzite structure and exhibit high c-axis orientation along the (002). No extra peaks were observed after addition of dopants into the ZnO matrix. This result shows that the samples are in the form of a single phase of ZnO. The position of the (002) diffraction peak for ZnO: 2%Y film shifts towards lower angles compared to that of pure ZnO, indicating that the lattice parameters of ZnO: 2%Y are larger than those of pure ZnO. This indicates that Y^{3+} ions are successfully incorporated into the ZnO lattice. The incorporation of Y is expected to expand the lattice parameters of ZnO, owing to the ionic radius difference between Y^{3+} ions (0.094 nm) and Zn^{2+} (0.074nm). Similar results have been reported by Kumar et al [31], for Y-doped ZnO prepared using a sol-gel route. When Li is introduced as codopant, the lattice parameters are expected to decrease because the ionic radius of Zn^{2+} (0.074 nm) is larger than that of Li^{+} (0.068 nm), and consequently the (002) shifts back to larger angles as observed in figure 1b. On the other hand, Boudjouan et al [32] reported an increase of the intensity of the (002) in Li doped ZnO thin films for Li concentrations between 5 and 15 at% that they attribute to an enhancement of the crystal

quality. In our samples, initially a decrease in the intensity is observed, however, as Li concentration increases, to values comparable to those used by Boudjouan, an increase in intensity of the (002) is also observed. Scherrer's formula [33] was used in order to determine the crystallite size of each sample from the full width at half maxima (FWHM) of the dominant diffraction peak, according to the equation:

$$D = \frac{0.9\,\lambda}{\beta\,cos\theta}$$

Where D, λ, θ and β correspond to the average crystallite size, X-ray wavelength, Bragg's diffraction angle and the full width at half maxim (FWHM) respectively. Figure 2 shows the variation of both lattice parameters and crystallite size with dopant concentration. It is observed that both lattice parameters decrease by increasing Li content (x) from x= 0 at.% to x= 5 at.%, although the ratio c/a remains at the same value for all doped and undoped samples, indicating that the hexagonal symmetry is well preserved upon doping. Since the ionic radius of Li^{+} (0.076 nm) is smaller than that of Y^{3+} (0.094 nm) and Zn^{+2} (0.074 nm), the substitution of an increasing number of larger ions could explain the observed decrease. On the other hand, it has been reported elsewhere that the decrease of crystallite size at low Li content was first attributed to its low solubility in the ZnO. In addition, Li can favour the appearance of nucleation sites, with the subsequent decrease in grain size [34].

Table 1 shows the interplanar spacing d_{hkl} and the lattice parameters for all samples, and the values of the micro-strain obtained by applying the following equation [35],

$$\varepsilon = \frac{\beta}{4tan\theta}$$

The surface morphology of the films was analyzed using SEM. Fig. 3 shows representative images of the films. All samples were continous and homogenous over large areas. The films are composed of particles, many of them showing hexagonal shapes, with sizes which depend on the concentration of dopants. The particles size of the films was estimated from direct measurements from the SEM images, table 2, taking

into consideration around 200 individual particles in each sample. The histograms of the different samples are shown in the figure 1 of the supporting information. As compared to undoped samples (a), it is clear that the particles size increases when zinc oxide is doped with yttrium (b) and then decreases by addition of 3 to 5 at% lithium (c, d), increasing again when 7% lithium is introduced (e).This trend is the same observed for the average crystallite size,(D) calculated from XRD which is also shown in table for comparison.

The optical properties of the films have been evaluated by means UV-Vis spectroscopy (transmission, absorption modes), photoluminescence and Raman spectroscopy.

The co-doped films present a high transparency close to the absorption edge compared to Y doped ZnO thin films (Fig. 4a). All the transmission spectra exhibited shoulders in the UV region, similar to those reported by Mimouni et al.[36]. The absorption measurements show a similar trend for pure, doped and co-doped ZnO films. In all cases, sharp absorption edges locate at approximately 375- 400 nm are observed (Fig. 4b).

The optical bandgap of the sprayed films was determined from the Tauc analysis. Fig. 5 shows the Tauc plot $(\alpha h\upsilon)^2$ as a function of (hν) for the different samples. The values of E_g are obtained from the extrapolation of the linear portion of this plot. For low Li co-doping, the optical band gap increases with respect to pure and ZnO: 2%Y films. Identical results have also been reported for Li doped ZnO thin films [37]. This E_g trend could be due to the Burstein-Moss effect. However, the increase of Li co-doping up to 5 and 7 at.% at fixed Y content was found to reduce the optical band gap value to 3.48 and 3.22 eV, respectively as shown in the figure 5-f. Nian et al.[27] reported similar behaviour by adding Li co-doping to Al doped ZnO films. This decrease in E_g, upon incorporation of these levels of Li, could also be explained by generation of new states within the forbidden zone near the valence and conduction bands. This phenomenon was initially described by Urbach [38] and Martienssen [39]. Following this analysis, the Urbach tail may be determined from the expression

$$\alpha = \alpha_0 e^{\frac{h\nu}{E_U}}$$

where α_0 is a constant, α represents the observed optical absorption and E_U is the Urbach energy. By plotting lnα as a function of (hν), the Urbach energy is the inverse of the slope. The obtained values for both optical bandgap and Urbach energy are grouped together in table 3 and displayed in figure 5-f for different thin films. It can be clearly observed that at low Li content the Urbach energy has increased with respect to those of pure and singly doped film ZnO: 2%Y, which indicates that the insertion of a low Li content in ZnO matrix generates crystalline disorder. The redistribution of the smaller Li atoms and the consequent lattice relaxation could be behind the decrease of the Urbach energy for the higher Li contents. This behavior is consistent with the enhancement of the crystallinity of the codoped films for higher Li contents already described from XRD analysis.

In order to investigate the quality of the as deposited films, we have studied the PL emissions of all the samples in the wavelength range of 350-750 nm. Fig.6a shows the PL spectra recorded at room temperature. The PL spectra of all films consist mainly of an intense UV near band edge emission (NBE) located at 386-394 nm and a weak deep level emission (DLE) band centered in the region around 650 nm. The weakness of the visible band emission confirms the high quality of the studied specimens. The structure of the NBE reflects the singularity of the films doped with the lowest Li content. As can be observed in figure 6b, doping with Y already causes a shift towards higher energy, when Li is introduced as codopant this shift increases, however for the lightest doping (sample 3Li), two components are clearly visible. The most intense centered around 390 nm and the second slightly above 400 nm close to the position observed in the films doped only with Y. By increasing the Li concentration, the NBE becomes narrower and, for both 5% and 7% Li, is centered about 400 nm, intermediate between Y doped and Y3Li sample. Besides, it can be found that the incorporation of a 3 at.% Li content gives rise to a small hump located at 525 nm, which was reported by Vanheusden et al.[40] and Egelhaaf et al.[41] as a typical band for ZnO materials ,the green band emission that disappeared for higher Li co-doping. The suppression of

the peak at around 525 nm could be related to the decrease of the density of defects in the films. The pure and ZnO: 2%Y films exhibit a broad visible emission band, centered at 650 nm, which can be attributed to the red emissions linked to O_i defects [42]. By Li codoping, the red band practically disappears, and only weak green band is observed for the 3Li sample, as has been already mentioned. The increase of the intensity observed above 700nm could be attributed to the tail of the second order of the UV band.

To further confirm the good crystallinity of the films, the I_{uv}/I_{vis} ratio were calculated, table 4. Note that the insertion of Li as co-dopant leads to an improvement of the crystalline quality of the films, when compared to pure and Y doped ZnO films. In fact, the improvement becomes optimum for a 5 at% Li addition.

The Raman scattering spectra were carried out at room temperature in order to investigate the influence of Li co-doping on the vibrational and structural properties of ZnO thin films. Fig.7 depicts the room temperature Raman spectra of pure and ZnO: 2%Y thin films in the range of 200-700 cm^{-1}. It is clear that all the films exhibit similar peaks, indicating the actual incorporation of both Y and Li into the ZnO host structure. No other peaks or impurities corresponding to Y and Li elements were detected. The peaks centered at 265, and 485 cm^{-1} correspond to Si (substrate), the peaks at 425, and 547 cm^{-1} correspond to E_2 (high) and A_1(LO) modes of ZnO, respectively. The hexagonal wurtzite phase was confirmed by the presence of the intense and broad E_2(high) mode at 425 cm^{-1}. It can be noticed that the E_2 (high) becomes stronger and much broader by increasing Li co-doping level up to 5 at.%. It is also observed that the E_2 (high) mode shifts towards lower frequencies. This shift can be assigned to the stress in the films [43]. Therefore, the absence of new phases or impurities after introducing the Li co-doping is consistent with the XRD results. In addition, the proper incorporation of doping and co-doping elements has been confirmed by the change of the intensity of the main Raman mode E_2 (high). In other words, the results obtained by Raman spectroscopy show that the lattice symmetry was only slightly influenced.

Conclusions

In summary, ZnO and ZnO: 2%Y: x%Li were successfully sprayed onto glass substrates at 450 °C. Their structural, morphological and optical properties were evaluated. XRD analysis evidences diffractions patterns of a ZnO wurtzite hexagonal structure highly oriented along [002], with absence of impurities or new phases. SEM images reveal the dominance of hexagonal shaped particles with sizes in the nanometer range. No cracks on large area of the films are observed. The optical transmission spectra show that all the films exhibit a high transmittance, above 80%, in the visible range. Moreover, the optical band gap is enhanced by adding Li as co-dopant with respect to both pure and Y-doped ZnO films. The optimum doping concentration of Li has been found to be 5%. The photoluminescence investigations reveal that the UV emission also increases with Li codoping, while the deep level emission is reduced. Raman spectra of the films confirm the formation of a wurtzite phase ZnO.

Acknowledgment

This work was supported by MINECO/FEDER (MAT 2016-81118-P and MAT 2015-65274-R). O. B. thanks Aula del Estrecho fellowship

Journal Pre-proof

References

[1] Z. Zang, X. Tang, Enhanced fluorescence imaging performance of hydrophobic colloidal ZnO nanoparticles by a facile method, J. Alloys Compd. 619 (2015) 98–101. doi:10.1016/j.jallcom.2014.09.072.

[2] C. Li, C. Han, Y. Zhang, Z. Zang, M. Wang, X. Tang, J. Du, Enhanced photoresponse of self-powered perovskite photodetector based on ZnO nanoparticles decorated CsPbBr 3 films, Sol. Energy Mater. Sol. Cells. 172 (2017) 341–346.

Journal Pre-proof

doi:10.1016/j.solmat.2017.08.014.

[3] C. Li, Z. Zang, C. Han, Z. Hu, X. Tang, J. Du, Y. Leng, K. Sun, Enhanced random lasing emission from highly compact CsPbBr3 perovskite thin films decorated by ZnO nanoparticles, Nano Energy. 40 (2017) 195–202. doi:10.1016/j.nanoen.2017.08.013.

[4] T. Minami, T. Miyata, K. Ihara, Y. Minamino, S. Tsukada, Effect of ZnO film deposition methods on the photovoltaic properties of ZnO-Cu2O heterojunction devices, Thin Solid Films. 494 (2006) 47–52. doi:10.1016/j.tsf.2005.07.167.

[5] K. Cheng, R. Jin, J. Liu, X. Liu, J. Liu, Z. Lu, Y. Liu, L. Guo, Z. Du, Patterned honeycomb-like ZnO cavities for Cu(In,Ga)Se 2 thin film solar cells with omnidirectionally enhanced light harvesting, Sol. Energy Mater. Sol. Cells. 170 (2017) 211–218. doi:10.1016/j.solmat.2017.06.011.

[6] S. Zang, Y. Wang, M. Li, W. Su, H. Zhu, X. Zhang, Y. Liu, Fabrication of efficient PbS colloidal quantum dot solar cell with low temperature sputter-deposited ZnO electron transport layer, Sol. Energy Mater. Sol. Cells. 169 (2017) 264–269. doi:10.1016/j.solmat.2017.05.026.

[7] H.S. Kim, F. Lugo, S.J. Pearton, D.P. Norton, Y.-L. Wang, F. Ren, Phosphorus doped ZnO light emitting diodes fabricated via pulsed laser deposition, Appl. Phys. Lett. 92 (2008) 112108.

[8] S.K. Patil, S.S. Shinde, K.Y. Rajpure, Physical properties of spray deposited Ni-doped zinc oxide thin films, Ceram. Int. 39 (2013) 3901–3907. doi:10.1016/j.ceramint.2012.10.234.

Journal Pre-proof

[9] X. Fang, Y. Bando, U.K. Gautam, T. Zhai, H. Zeng, X. Xu, M. Liao, D. Golberg, ZnO and ZnS Nanostructures: Ultraviolet-Light Emitters, Lasers, and Sensors, Crit. Rev. Solid State Mater. Sci. 34 (2009) 190–223. doi:10.1080/10408430903245393.

[10] N. Kumaresan, K. Ramamurthi, R. Ramesh Babu, K. Sethuraman, S. Moorthy Babu, Hydrothermally grown ZnO nanoparticles for effective photocatalytic activity, Appl. Surf. Sci. 418 (2017) 138–146. doi:10.1016/j.apsusc.2016.12.231.

[11] A.H. Zyoud, M. Dwikat, S. Al-Shakhshir, S. Ateeq, J. Ishtaiwa, M.H.S. Helal, M. Kharoof, S. Alami, H. Kelani, G. Campet, H.S. Hilal, ZnO nanoparticles in complete photo-mineralization of aqueous gram negative bacteria and their organic content with direct solar light, Sol. Energy Mater. Sol. Cells. 168 (2017) 30–37. doi:10.1016/j.solmat.2017.04.006.

[12] L. Liu, W. Chen, Y. Li, Author ' s Accepted Manuscript, J. Memb. Sci. (2015). doi:10.1016/j.memsci.2015.12.065.

[13] D. Nesheva, V. Dzhurkov, I. Stambolova, V. Blaskov, I. Bineva, J.M. Calderon Moreno, S. Preda, M. Gartner, T. Hristova-Vasileva, M. Shipochka, Surface modification and chemical sensitivity of sol gel deposited nanocrystalline ZnO films, Mater. Chem. Phys. 209 (2018) 165–171. doi:10.1016/j.matchemphys.2018.01.074.

[14] A. Moulahi, F. Sediri, ZnO nanoswords and nanopills: Hydrothermal synthesis, characterization and optical properties, Ceram. Int. 40 (2014) 943–950. doi:10.1016/j.ceramint.2013.06.090.

[15] V.K. Ashith, G.K. Rao, S.N. Moger, S. R, Effect of post-deposition annealing on the properties of ZnO films obtained by high temperature, micro-controller based SILAR

Journal Pre-proof

deposition, Ceram. Int. 44 (2018) 10669–10676. doi:10.1016/j.ceramint.2018.03.097.

[16] Z.E. Vakulov, E.G. Zamburg, D.A. Khakhulin, O.A. Ageev, Thermal stability of ZnO thin films fabricated by pulsed laser deposition, Mater. Sci. Semicond. Process. 66 (2017) 21–25. doi:10.1016/j.mssp.2017.03.006.

[17] M. Hjiri, M.S. Aida, O.M. Lemine, L. El Mir, Study of defects in Li-doped ZnO thin films, Mater. Sci. Semicond. Process. 89 (2019) 149–153. doi:10.1016/j.mssp.2018.09.010.

[18] A. Mondal, S. Pal, A. Sarkar, T.S. Bhattacharya, A. Das, N. Gogurla, S.K. Ray, P. Kumar, D. Kanjilal, K.D. Devi, A. Singha, S. Chattopadhyay, D. Jana, Raman spectroscopic analysis on Li, N and (Li,N) implanted ZnO, Mater. Sci. Semicond. Process. 80 (2018) 111–117. doi:10.1016/j.mssp.2018.02.026.

[19] Y.K. Park, J.I. Han, M.G. Kwak, H. Yang, S.H. Ju, W.S. Cho, Time-resolved spectroscopic study of energy transfer in ZnO:EuCl3 phosphors, J. Lumin. 78 (1998) 87–90. doi:10.1016/S0022-2313(97)00277-9.

[20] S. Heo, S.K. Sharma, S. Lee, Y. Lee, C. Kim, B. Lee, H. Lee, D.Y. Kim, Effects of y contents on surface, structural, optical, and electrical properties for Y-doped ZnO thin films, Thin Solid Films. 558 (2014) 27–30. doi:10.1016/j.tsf.2014.02.025.

[21] M. Gao, J. Yang, L. Yang, Y. Zhang, J. Lang, H. Liu, H. Fan, Y. Sun, Z. Zhang, H. Song, Enhancement of optical properties and donor-related emissions in Y-doped ZnO, Superlattices Microstruct. 52 (2012) 84–91. doi:10.1016/j.spmi.2012.03.016.

Journal Pre-proof

[22] X. Han, K. Han, M. Tao, Low Resistivity Yttrium-Doped Zinc Oxide by Electrochemical Deposition, J. Electrochem. Soc. 157 (2010) H593. doi:10.1149/1.3377092.

[23] L. li Yang, J. hai Yang, D. dan Wang, Y. jun Zhang, Y. xin Wang, H. lian Liu, H. gang Fan, J. hui Lang, Photoluminescence and Raman analysis of ZnO nanowires deposited on Si(1 0 0) via vapor-liquid-solid process, Phys. E Low-Dimensional Syst. Nanostructures. 40 (2008) 920–923. doi:10.1016/j.physe.2007.11.025.

[24] R. Kaur, A. V. Singh, R.M. Mehra, Structural, electrical and optical properties of sol-gel derived yttrium doped ZnO films, Phys. Status Solidi. 202 (2005) 1053–1059. doi:10.1002/pssa.200420006.

[25] S.K. Sharma, D.Y. Kim, Microstructure and Optical Properties of Yttrium-doped Zinc Oxide (YZO) Nanobolts Synthesized by Hydrothermal Method, J. Mater. Sci. Technol. 32 (2016) 12–16. doi:10.1016/j.jmst.2015.11.001.

[26] J. Yang, R. Wang, L. Yang, J. Lang, M. Wei, M. Gao, X. Liu, J. Cao, X. Li, N. Yang, Tunable deep-level emission in ZnO nanoparticles via yttrium doping, J. Alloys Compd. 509 (2011) 3606–3612. doi:10.1016/j.jallcom.2010.12.102.

[27] H. Nian, S.H. Hahn, K.K. Koo, J.S. Kim, S. Kim, E.W. Shin, E.J. Kim, Preparation and characterization of sol-gel Li and Al codoped ZnO thin films, Mater. Lett. 64 (2010) 157–160. doi:10.1016/j.matlet.2009.10.030.

[28] S. Fujihara, C. Sasaki, T. Kimura, E ects of Li and Mg doping on microstructure and properties of sol-gel ZnO thin lms, J. Eur. Ceram. Soc. 21 (2001) 2109–2112.

[29] M. Caglar, Y. Caglar, S. Aksoy, S. Ilican, Temperature dependence of the optical

Journal Pre-proof

band gap and electrical conductivity of sol-gel derived undoped and Li-doped ZnO films, Appl. Surf. Sci. 256 (2010) 4966–4971. doi:10.1016/j.apsusc.2010.03.010.

[30] O. Bazta, A. Urbieta, J. Piqueras, P. Fernández, M. Addou, J.J. Calvino, A.B. Hungría, Influence of yttrium doping on the structural, morphological and optical properties of nanostructured ZnO thin films grown by spray pyrolysis, (2018). doi:10.1016/j.ceramint.2018.12.178.

[31] P. Kumar, V. Singh, V. Sharma, G. Rana, H.K. Malik, K. Asokan, Investigation of phase segregation in yttrium doped zinc oxide, Ceram. Int. 41 (2015) 6734–6739. doi:10.1016/j.ceramint.2015.01.117.

[32] F. Boudjouan, A. Chelouche, T. Touam, D. Djouadi, R. Mahiou, G. Chadeyron, A. Fischer, A. Boudrioua, Doping effect investigation of Li-doped nanostructured ZnO thin films prepared by sol–gel process, J. Mater. Sci. Mater. Electron. 27 (2016) 8040–8046. doi:10.1007/s10854-016-4800-2.

[33] P. Kumar, H.K. Malik, A. Ghosh, R. Thangavel, K. Asokan, Bandgap tuning in highly c-axis oriented Zn1− xMgxO thin films, Appl. Phys. Lett. 102 (2013) 221903.

[34] S.D. Senol, M. Erdem, Hydrothermal synthesis of Li co-doped Zn0.98Mg0.02O nanoparticles and their structural, optical and electrical properties, Ceram. Int. 42 (2016) 10929–10934. doi:10.1016/j.ceramint.2016.03.227.

[35] P.P. Sahay, R.K. Nath, Al-doped ZnO thin films as methanol sensors, Sensors Actuators, B Chem. 134 (2008) 654–659. doi:10.1016/j.snb.2008.06.006.

[36] R. Mimouni, O. Kamoun, A. Yumak, A. Mhamdi, K. Boubaker, P. Petkova, M.

Journal Pre-proof

Amlouk, Effect of Mn content on structural, optical, opto-thermal and electrical properties of ZnO:Mn sprayed thin films compounds, J. Alloys Compd. 645 (2015) 100–111. doi:10.1016/j.jallcom.2015.05.012.

[37] P. Chand, A. Gaur, A. Kumar, U.K. Gaur, Structural, morphological and optical study of Li doped ZnO thin films on Si (100) substrate deposited by pulsed laser deposition, Ceram. Int. 40 (2014) 11915–11923. doi:10.1016/j.ceramint.2014.04.027.

[38] F. Urbach, The long-wavelength edge of photographic sensitivity and of the electronic absorption of solids, Phys. Rev. 92 (1953) 1324.

[39] W. Martienssen, W. Martienssen, J. Phys. Chem. Solids 2, 257 (1957), J. Phys. Chem. Solids. 2 (1957) 257.

[40] K. Vanheusden, C.H. Seager, W.L. t Warren, D.R. Tallant, J.A. Voigt, Correlation between photoluminescence and oxygen vacancies in ZnO phosphors, Appl. Phys. Lett. 68 (1996) 403–405.

[41] H.J. Egelhaaf, D. Oelkrug, Luminescence and nonradiative deactivation of excited states involving oxygen defect centers in polycrystalline ZnO, J. Cryst. Growth. 161 (1996) 190–194. doi:10.1016/0022-0248(95)00634-6.

[42] A.F. Kohan, G. Ceder, D. Morgan, C.G. Van de Walle, First-principles study of native point defects in ZnO, Phys. Rev. B. 61 (2000) 15019–15027. doi:10.1103/PhysRevB.61.15019.

[43] X.Q. Gu, L.P. Zhu, Z.Z. Ye, H.P. He, Y.Z. Zhang, B.H. Zhao, Preparation of Li and Er

codoped ZnO thin films and their photoluminescence, Thin Solid Films. 517 (2009)

5134–5136. doi:10.1016/j.tsf.2009.03.004.

Fig. 1. a) XRD patterns of (Y,Li) co-doped ZnO sprayed thin films. b) Variation of (002) peak position of pure ZnO and samples with extreme lithium content (ZnO:2Y and ZnO: 2Y: 7Li)

Fig. 2. Variation of Lattice parameters (a & c) and crystallite size D versus Y-Li concentrations.

Fig. 3. (a,b) FESEM images of pure and ZnO: 2Y; (c) FESEM images of ZnO: 2Y: 3Li; (d) FESEM images of ZnO: 2Y: 5Li; (e) FESEM images of ZnO: 2Y: 7Li.

Fig. 4. a) Spectral transmission characteristics of undoped and Li/Y doped ZnO thin films **.** b) Absorbance spectra of pure and Li/Y doped ZnO thin films.

Fig. 5. (a-f) $(\alpha h\nu)^2$ versus $h\nu$ plots of undoped and ZnO: (Y/Li) sprayed films and (f) variation of E_g and E_u versus Y and Li levels.

Fig. 6a. Room temperature PL spectra of the (Li /Y) co-doped ZnO thin films.

Fig. 6b. Enlarged spectra of different films from 350 nm to 450 nm.

Fig. 7. Raman spectra of thin films ZnO deposited at different doping and co-doping levels.

Table 1 Structural parameters of pure doped and co-doped ZnO thin films.

Sample	Lattice parameters		Interplanar spacing d_{hkl}		Microstrain ε (10^{-4}) (±5.5%)
	a=b (Å)	c (Å)	d_{100} (Å)	d_{002} (Å)	
ZnO	3.24	5.20	2.81	2.60	13.7
ZnO: 2Y	3.26	5.22	2.82	2.61	13.6
ZnO: 2Y: 3Li	3.25	5.20	2.82	2.60	26.07
ZnO: 2Y: 5Li	3.24	5.20	2.81	2.60	29.00
ZnO: 2Y: 7Li	3.25	5.20	2.81	2.60	23.95

Table 2 Particle size values from both Scherrer's law and SEM investigations.

Journal Pre-proof

Sample	Particle size (nm) Scherrer	Particle size (nm) FESEM
ZnO	48	116
ZnO: 2Y	49	140
ZnO: 2Y: 3Li	44	132
ZnO: 2Y: 5Li	40	119
ZnO: 2Y: 7Li	49	160

Table 3 Calculated values of optical band gap and Urbach energy.

Sample	E_g(eV)	E_u(meV)
ZnO	3.12	103.90
ZnO: 2Y	3.14	100.47
ZnO: 2Y: 3Li	3.58	216.82
ZnO: 2Y: 5Li	3.48	152.27
ZnO: 2Y: 7Li	3.22	93.99

Table 4 Effect of the doping and co-doping elements on ZnO quality.

Sample	ZnO	ZnO: 2Y	ZnO: 2Y: 3Li	ZnO: 2Y: 5Li	ZnO: 2Y: 7Li
I_{uv}/I_{vis}	2.82 ±0.05	3.16 ±0.05	9.32 ±0.05	29.86 ±0.05	19.87 ±0.05

Journal Pre-proof

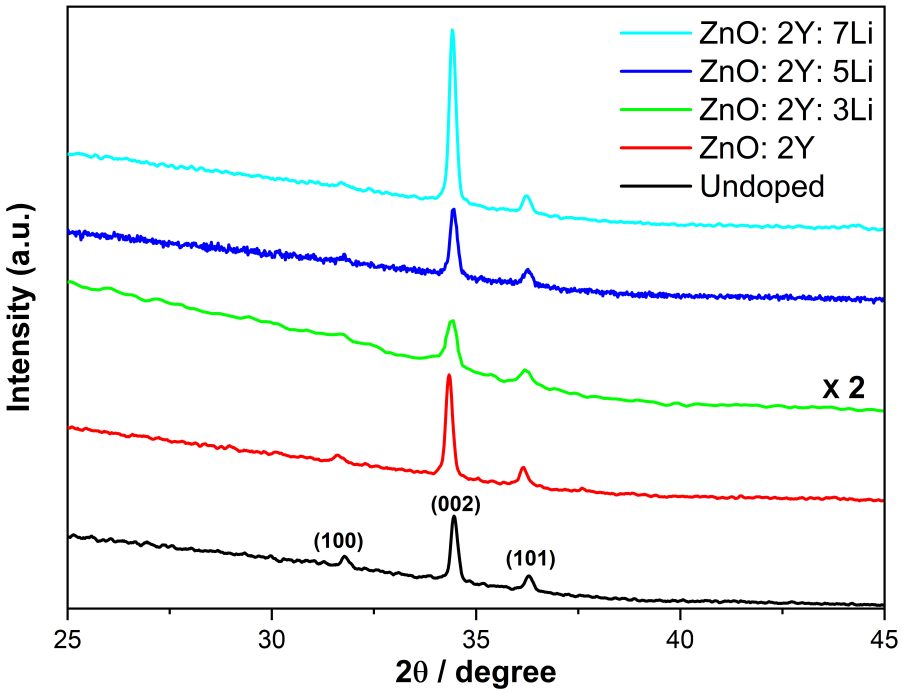
ZnO: 2Y: 7Li
ZnO: 2Y: 5Li
ZnO: 2Y: 3Li
ZnO: 2Y
Undoped
x 2
(002)
(100)
(101)
Intensity (a.u.)
25
30
35
40
45
2θ / degree

Figure 1a

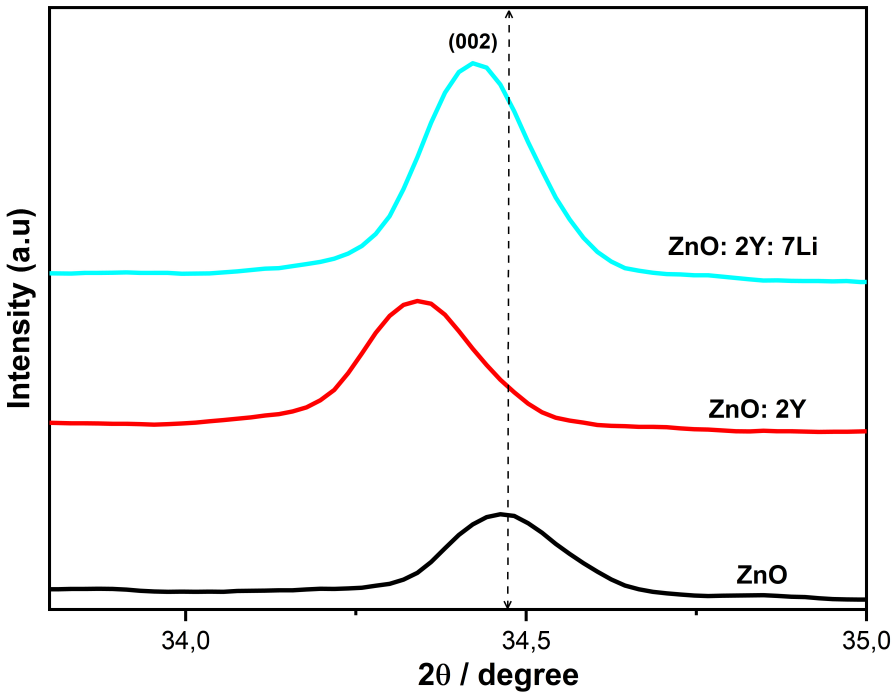

Figure 1b

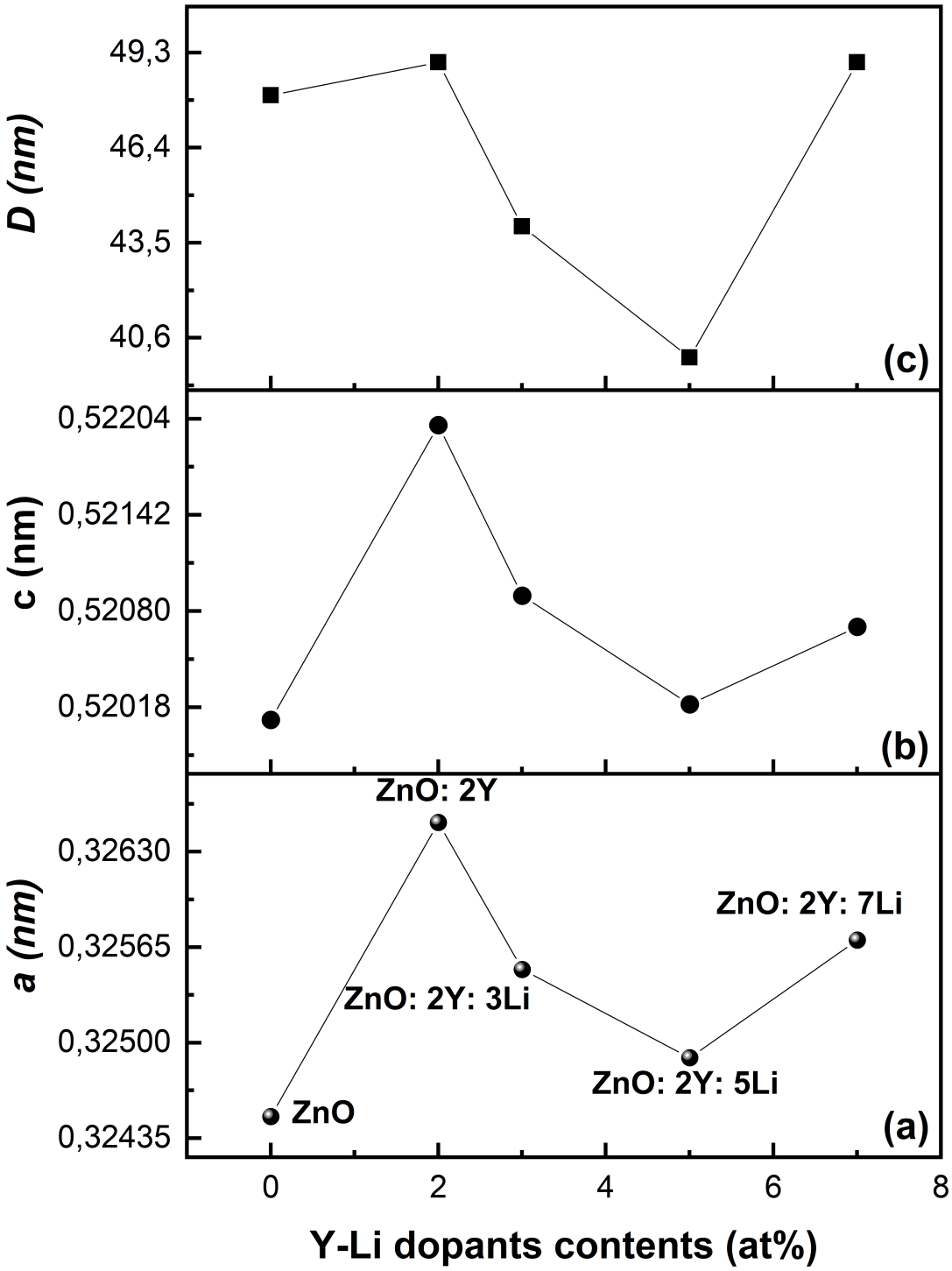
D (nm)
49,3
46,4
43,5
40,6
(c)
c (nm)
0,52204
0,52142
0,52080
0,52018
(b)
a (nm)
0,32630
0,32565
0,32500
0,32435
ZnO: 2Y
ZnO: 2Y: 7Li
ZnO: 2Y: 3Li
ZnO: 2Y: 5Li
ZnO
(a)
0
2
4
6
8
Y-Li dopants contents (at%)

Figure 2

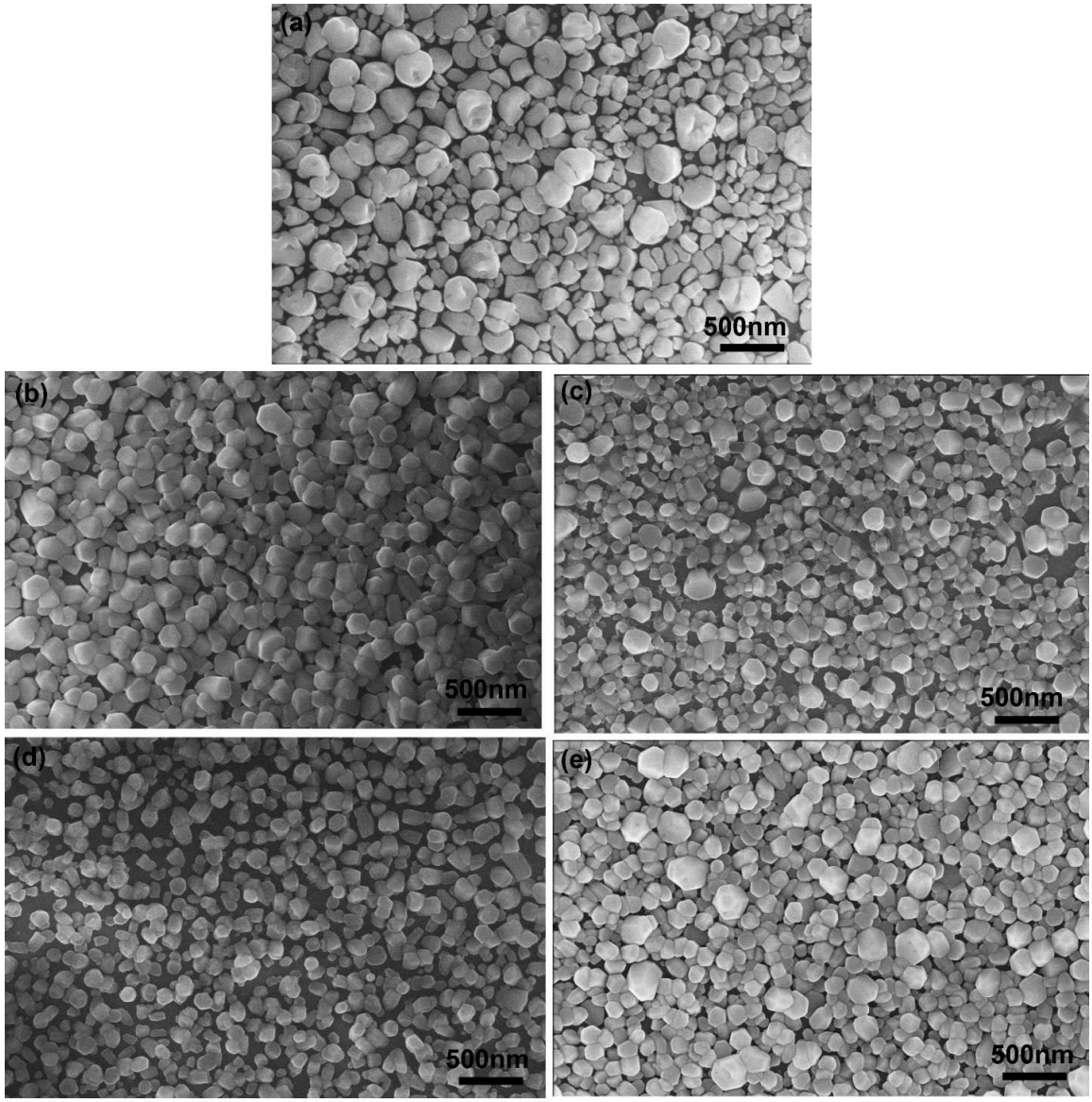

Figure 3

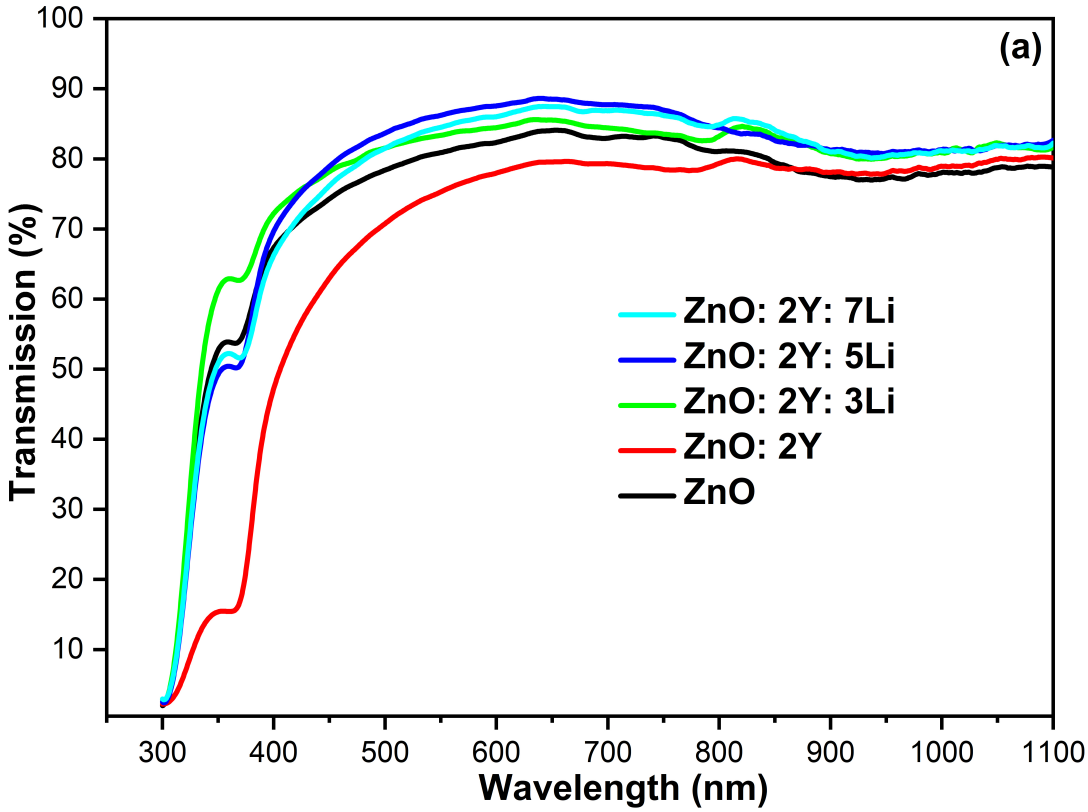
(a)
Transmission (%)
Wavelength (nm)
ZnO: 2Y: 7Li
ZnO: 2Y: 5Li
ZnO: 2Y: 3Li
ZnO: 2Y
ZnO
100
90
80
70
60
50
40
30
20
10
300
400
500
600
700
800
900
1000
1100

Figure 4a

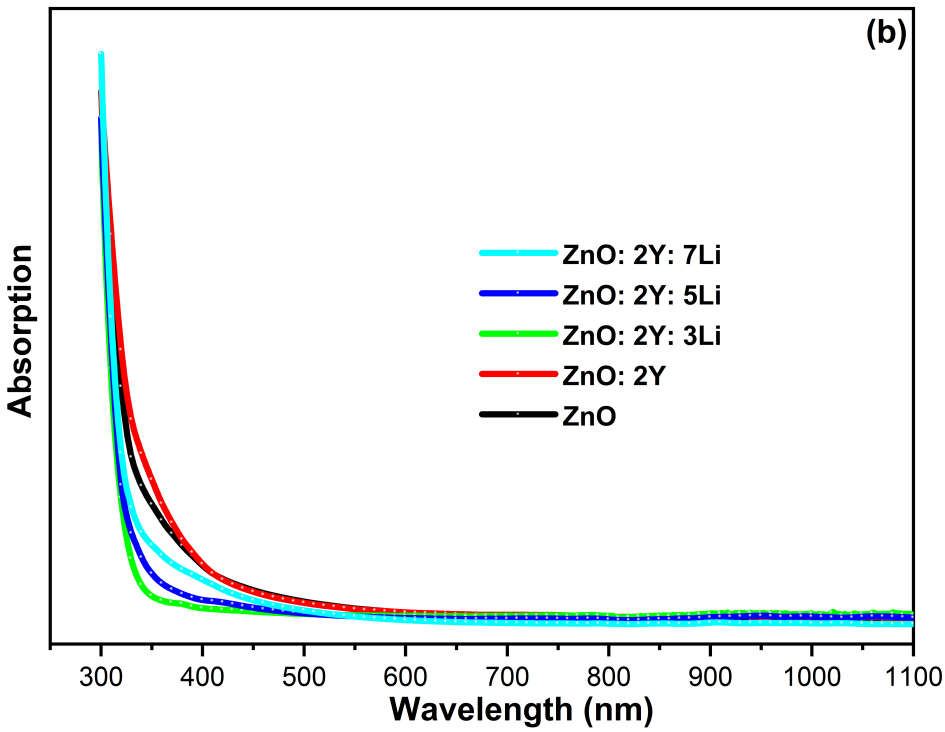

Figure 4b

Journal

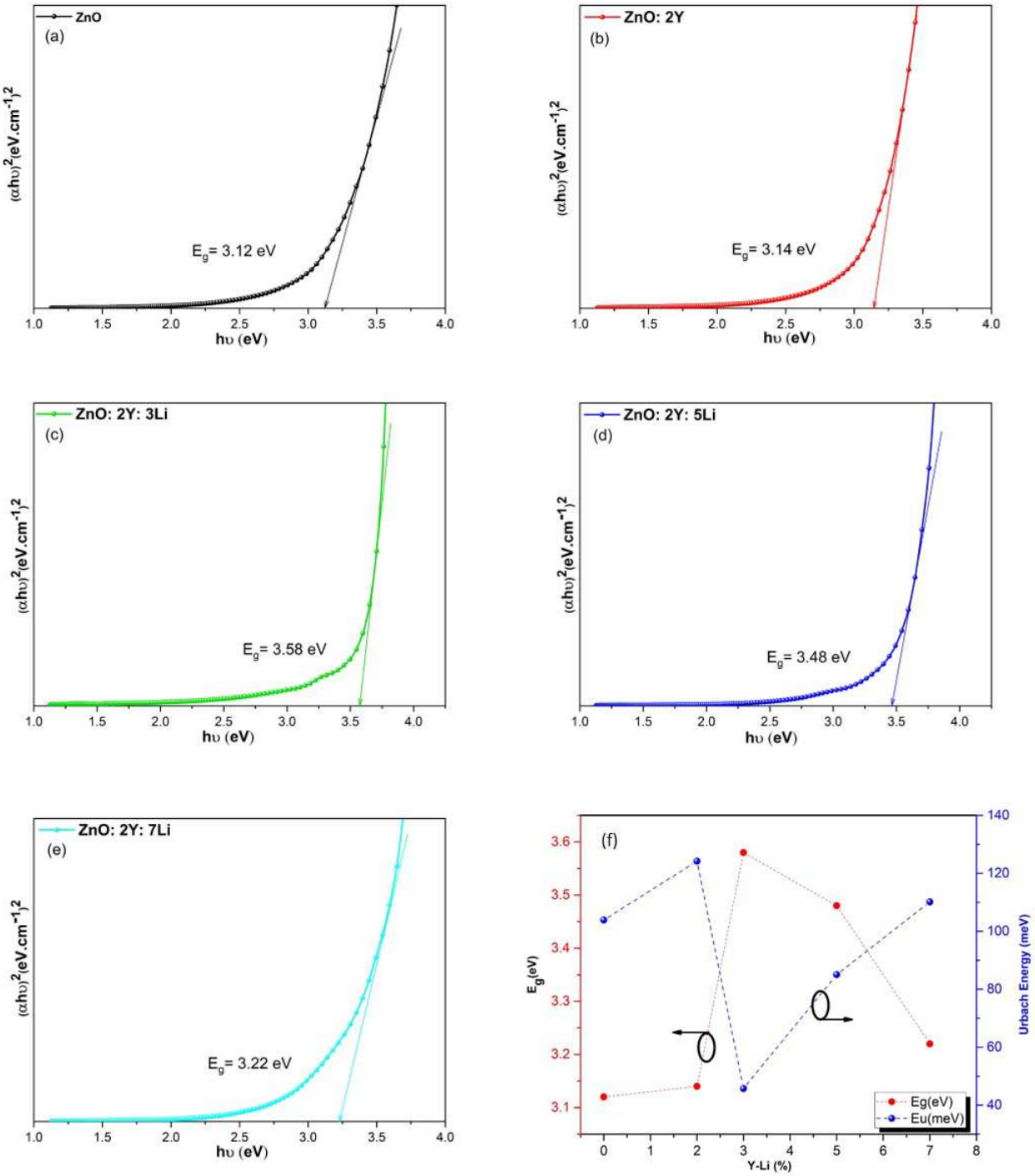
ZnO
(a)
E_g= 3.12 eV
ZnO: 2Y
(b)
E_g= 3.14 eV
ZnO: 2Y: 3Li
(c)
E_g= 3.58 eV
ZnO: 2Y: 5Li
(d)
E_g= 3.48 eV
ZnO: 2Y: 7Li
(e)
E_g= 3.22 eV
$(\alpha h\upsilon)^2$(eV.cm^{-1})^2
hυ (eV)
(f)
E_g(eV)
Urbach Energy (meV)
Y-Li (%)
Eg(eV)
Eu(meV)

Figure 5

Figure 6a

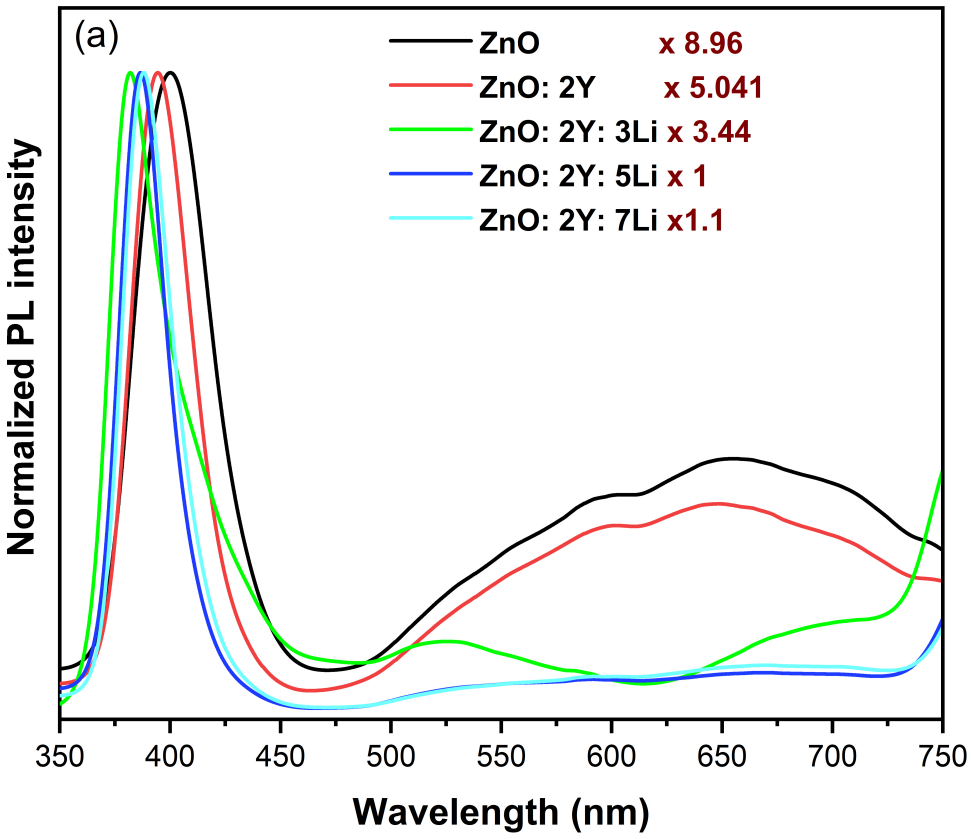
(a)
ZnO x 8.96
ZnO: 2Y x 5.041
ZnO: 2Y: 3Li x 3.44
ZnO: 2Y: 5Li x 1
ZnO: 2Y: 7Li x1.1
Normalized PL intensity
350
400
450
500
550
600
650
700
750
Wavelength (nm)

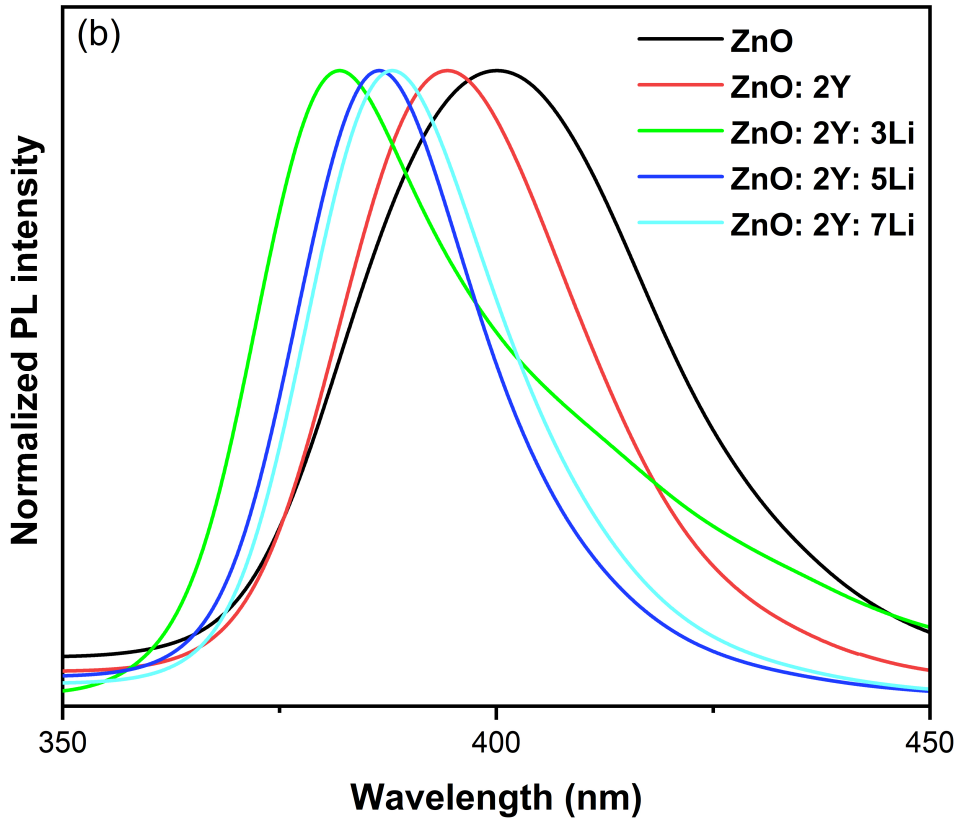
(b)
ZnO
ZnO: 2Y
ZnO: 2Y: 3Li
ZnO: 2Y: 5Li
ZnO: 2Y: 7Li
Normalized PL intensity
350
400
450
Wavelength (nm)

Figure 6b

Figure 7

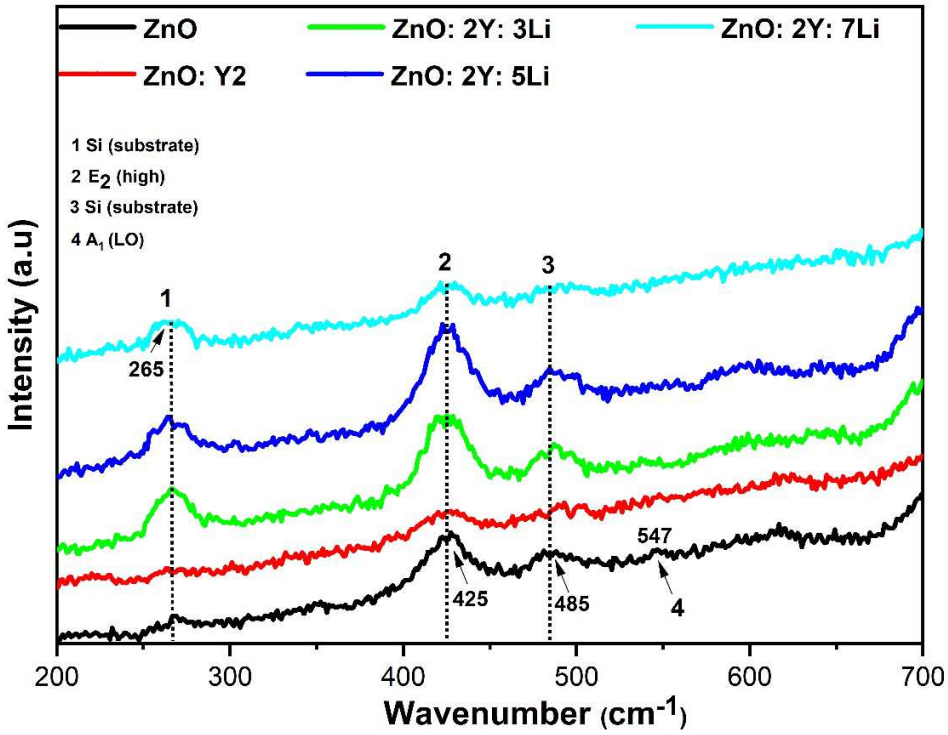
ZnO
ZnO: 2Y: 3Li
ZnO: 2Y: 7Li
ZnO: Y2
ZnO: 2Y: 5Li
1 Si (substrate)
2 E2 (high)
3 Si (substrate)
4 A1 (LO)
Intensity (a.u)
Wavenumber (cm-1)
200
300
400
500
600
700
1
2
3
4
265
425
485
547

Journal Pre-proof

Highlights

- ZnO and (ZnO: 2%Y: x%Li) (x=0, 3, 5 and 7 at. %) obtained by spray pyrolysis.
- No peaks corresponding to the dopants phases or impurities phases were detected.
- Co-doped films present a high transparency compared to mono-doped thin films.
- UV emission intensity was markedly enhanced after Li incorporation.
- The present system suggest its potential application in optoelectronic devices.

Journal Pre-proof